Chapter 1

Introduction

1.1 Elementary properties of quantum dots

Quantum dots (QDs) can be defined as solid-state structures capable of confining electrons and holes in all spatial directions. They are frequently modelled as three-dimensional wells of confining potential, or "quantum boxes" (usually with walls of finite height); the confinement is usually produced electrostatically or by appropriate material engineering. Typical dimensions of QDs range from a few to several hundreds of nanometres, which results in distinct quantisation of the single-particle energy spectrum of trapped carriers: the energy gaps between levels are typically of the order of several microelectronvolts to several tens of millielectronvolts (meV). At this point one frequently draws an analogy between the QDs and atoms, in which electrons are confined by the positive potential of the nucleus, and their energy levels form well-separated shells. This analogy is quite useful, and QDs are often called "artificial atoms" [8, 62]. Indeed, as mentioned before, in QDs, as in atoms, the wave functions of charge carriers are confined in the vicinity of the dot centre, and the corresponding eigenenergies form a discrete spectrum. If the QD is of a sufficiently high symmetry, these levels can form shells with increasing degeneracy. Also, it is possible to obtain dots with well-controllable number of confined carriers, from one to

hundreds, and indeed reproduce a Mendeleev periodic table of "QD elements" [32, 121]. The carriers can relax or be promoted from one level to another subject to selection rules similar to those found in atoms. There are, however, notable differences between the artificial atoms and their natural counterparts. First of all, quantum dots can confine holes as well as electrons, while the positive potential of atomic nucleus can only confine the negative carriers. Further, the lateral confinement in QDs is usually smooth, and in many cases approximately parabolic, in contrast to the Coulomb potential of atoms, possessing a singularity at the nucleus. Also, QDs are composed of thousands of atoms or more. This size leads to a smaller interlevel separation (tens of meV at most), compared to that of atoms, where the shells are separated by a few eV. Moreover, the lateral confinement (Coulomb potential) in atoms is fixed and defined by the electrostatic charge of the nucleus, which makes it difficult to change the number of electrons confined by it. In contrast, in certain types of dots the QD lateral confinement can be tuned, and the same device can contain from zero to hundreds of confined electrons (I shall discuss these devices later on).

The first successful attempts at creating QDs date back to the early 1980's [62]. Since then fabrication technologies have progressed rapidly, and today it is possible to manufacture dots of various shapes and sizes, and to tailor almost all the properties indicated above. It is then not surprising that QDs have become an area of interest both in the domain of fundamental research and device physics. This thesis will cover in detail only a small section of this ever-increasing field. For the reader interested in a general introduction to QDs, QD devices and terminology in their full variety I suggest three books: by Bimberg, Grundmann, and Ledentsov [20], Jacak, Hawrylak, and Wójs [62], and Michler [85], and review articles by Ashoori [8], Kastner [65], and Chakraborty [30].

1.2 Quantum-dot density of states

Control over the number of confined carriers seems to be of particular importance in the physics of quantum dots. Therefore, many important realisations of QDs employ semiconductor structures, where the number of mobile carriers can be controlled by means of appropriate doping, illumination, etc., and this work will focus on such structures exclusively. For this reason, at this point I will introduce an alternative treatment of the QD energy quantisation using the language of the density of states (DOS). At the same time, the notion of "zero-dimensional states" is presented here more rigorously and put in context of other structures with reduced dimensionality, such as quantum wells and wires. The description given in this Section is similar to that presented in Ref. [62].

In my simplified description of the influence of the reduced dimensionality on DOS I shall assume my semiconductor materials to be isotropic, with parabolic energy bands and spherical energy isosurfaces, and I shall consider the electrons in conduction bands only. In this case, in order to calculate the DOS as a function of the wave vector k I will consider the number of electronic states $n(k)$ contained in an infinitesimal region $d^m k$ at the wave vector $\mathbf{k}$, where $m = 3$, 2 or 1 is the dimensionality of the material (the case of zero-dimensional structures will be considered separately). The DOS will be then calculated as [7]

$$\mathrm{DOS}(k) = \frac{dn(k)}{dk}. \tag{1.1}$$

This expression may contain an extra factor of two if the spin degeneracy of levels is taken into account.

Usually the DOS is calculated as a function of energy in the band, and to make contact with this formulation, I shall make use of the well-known formula for energy as a function of the wave vector:

$$E(k) = \frac{\hbar^2 k^2}{2m^*}, \tag{1.2}$$

where m^* is the effective mass of the electron, and k is the length of the wave vector $\mathbf{k}$.

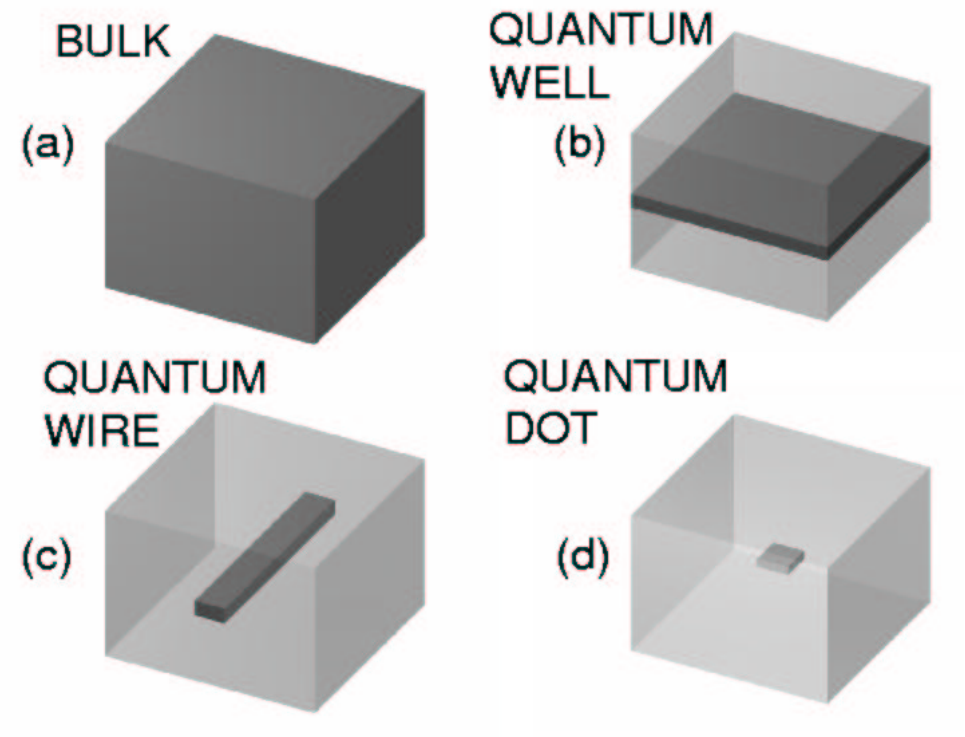

Figure 1.1: Four semiconductor structures of different dimensionality: bulk (a), quantum well (b), quantum wire (c), and quantum dot (d). The narrower (wider)-bandgap material is marked by the dark (light) colour

By combining the two formulae one can calculate

$$\mathrm{DOS}(E) = \frac{dn(E)}{dE}. \tag{1.3}$$

Let us now consider four semiconductor structures, presented in Figure 1.1. Part (a) of this Figure shows a macroscopic sample of bulk semiconductor material. If the dimensions of this sample are infinite, the single-particle energy spectrum in the conduction and the valence bands is continuous, and spherical coordinates can be introduced in Eq. (1.1). Thus the function $n(k)$ gives the number of states contained between two spherical surfaces, one with radius k, and another, with radius $k + dk$, and is

$$n^{3D}(k) = \frac{1}{(2\pi)^3} 4\pi k^2 dk. \tag{1.4}$$

As a result, the DOS as a function of energy in the band attains a well-known square-root form:

$$\mathrm{DOS}^{3D}(E) = \frac{1}{(2\pi)^2}\left(\frac{2m^*}{\hbar^2}\right)^{3/2}\sqrt{E}. \tag{1.5}$$

The energy as a function of the electronic wave vector k is shown in the left-hand panel, and the DOS as a function of energy - in the right-hand panel of Fig. 1.2 (a). Finite dimensions of the sample introduce boundary conditions resulting in quantisation of energy levels, but if the dimensions are sufficiently large, the spacing of levels is very small. The spectrum becomes quasi-continuous, and the changes to DOS are negligible.

If a layer of a narrower-bandgap material is sandwiched between two thick layers of a wider-bandgap material, one creates a quantum well, shown in Fig. 1.1 (b). If the edge of the conduction band in the well material is below the band edge of the barrier, the mobile carriers in the structure are trapped inside the well. They are still free to move in the plane, but their motion across the structure is strongly quantised. Thus the energy spectrum consists of distinct quantum-well energy levels E_0, E_1, ..., on top of which there is a quasi-continuous spectrum corresponding to the planar motion. In the left-hand panel of Fig. 1.2 (b) I show this energy spectrum as a function of the in-plane wave vector. In this case the function $n(k)$ describes the number of states of each subband contained between two circular boundaries, one with the radius k, and the other with the radius $k + dk$, and is

$$n^{2D}(k) = \frac{1}{(2\pi)^2}2\pi k dk. \tag{1.6}$$

The resulting total DOS of the quantum well is zero for energies below E_0, and then exhibits a steplike dependence on energy, with steps beginning at energies E_i, i.e., the quantum-well subband edges:

$$\mathrm{DOS}^{2D}(E) = \sum_i \frac{1}{2\pi}\frac{m^*}{\hbar^2}H(E - E_i), \tag{1.7}$$

where the Heaviside's function $H(x) = 1$ for $x \geq 0$ and 0 otherwise, and i enumerates the quantum-well subbands. This DOS is shown in the right-hand panel of Fig. 1.2 (b).

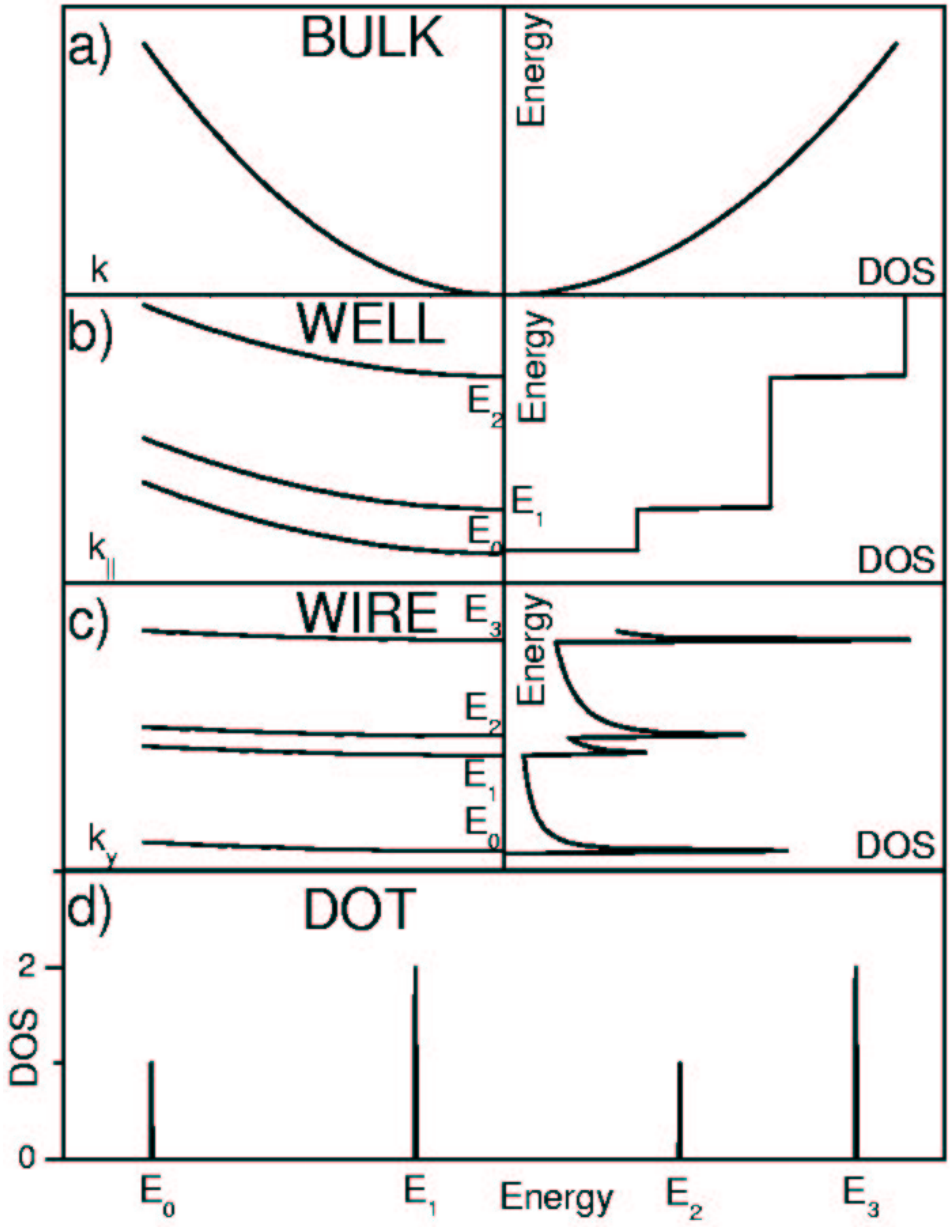

Figure 1.2: Energy as a function of wave vector (left-hand panels) and the density of states as a function of energy in the conduction band (right-hand panels) of a bulk material (a), quantum well (b), and quantum wire (c). The vertical axis shows the energy, while the horizontal axes - the length of the wave vector or the density of states, respectively. The density of states of a quantum dot is also shown (d)

A quantum wire, shown schematically in Fig. 1.1(c), is formed when the motion of the carriers is restricted in two directions, while they are free to move along the third direction (say, along the y axis). The electronic energy spectrum consists now of a ladder of discrete quantum-wire modes, on top of which there is a quasi-continuous one-dimensional spectrum corresponding to the motion along the wire. I show this spectrum as a function of the electronic wave vector in the left-hand panel of Fig. 1.2 (c). In this case the function $n(k)$ for each subband describes the number of states contained in a one-dimensional section of the reciprocal space between the wave vector k and $k + dk$, and is

$$n^{1D}(k) = \frac{1}{2\pi} dk. \tag{1.8}$$

The total quantum-wire DOS consists of a series of inverse-square-root peaks centered at the edges of the quantum-wire subbands:

$$\mathrm{DOS}^{1D}(E) = \sum_i \frac{1}{4\pi} \left(\frac{2m^*}{\hbar^2}\right)^{1/2} \frac{1}{\sqrt{(E - E_i)}} H(E - E_i). \tag{1.9}$$

This function is shown in the right-hand panel of Fig. 1.2 (c).

Finally, the zero-dimensional structure - a QD - is created when the well material is surrounded by the barrier on all sides, as shown in Fig. 1.1 (d). Here the electronic spectrum consists of discrete states, and the DOS is composed of delta function peaks at the QD energies; the height of these peaks corresponds to the degeneracy of the levels. In Fig.1.2 (d) I show a QD DOS for a dot whose base is a square and height is small compared to the lateral dimension. Due to this dimensional disparity, the energy scale introduced by the stronger, vertical quantisation will be different from that due to the lateral confinement: one expects a ladder of widely spaced vertical energy levels, on top of which there are the modes of the lateral motion, still discrete, but spaced much more closely. In fact, if the QD height is sufficiently small, the energy of the second vertical subband is already above the barrier, so the bound states contain the lowest vertical mode only. Furthermore, due to the square symmetry of the QD base, one expects the first excited state of this system to be doubly degenerate, which is reflected in the height

of the corresponding delta peak in Fig. 1.2 (d). This schematic picture is, of course, only valid in the region of energies corresponding to the QD bound states (below the barrier). Energies above the barrier correspond to the continuum states. At this point one might compare the DOS of these propagating states to that of the bulk material. Indeed, the wave functions of the states above the barrier will be distorted by the presence of the QD, but these distortions do not lead to major changes in the square-root dependence of the DOS on energy. Of particular interest is the case in which the wave function is distorted just so that its part inside the QD fits smoothly to the undistorted function in the barrier. If interrogated outside the QD, the state behaves then as if there was no QD at all (in other words, the scattering cross-section of the QD for this particular energy is zero). This is the Ramsauer-Townsend effect [110], well known in scattering theory, and the propagating states with this property are called resonances. These resonances can be thought of as an "echo" of the QD potential, experienced by the states above the barrier, and their corresponding wave functions must carry symmetries characteristic for the QD. They are of interest in device physics, and in particular in quantum-dot infrared photodetectors, briefly mentioned in the next section.

1.3 Fabrication of quantum dots

This Thesis is devoted to presenting my theoretical understanding of many-body systems confined by the potential of nanostructures. I would like to apply my theories to real systems, and obtain experimental verification of my results. To this end it is necessary to model the behaviour of the particles in realistic, experimentally attainable confinements. Perhaps the best way to understand the most important properties of these confinements is to present the techniques of nanostructure fabrication. In two decades of technological progress in this area several such techniques were developed. The starting point in some of them is a semiconductor quantum well (see Fig. 1.1(b)). One can further process

such a sample with lithography and etching to obtain free-standing nanopillars with a small amount of quantum well material located somewhere along their height [38, 103]. One can also evaporate an array of miniature metallic electrodes onto the surface, and subsequently polarise them with voltage - the resulting electrostatic field propagates down to the quantum well layer and creates the lateral confinement [115]. The third method here would involve a selective illumination of the surface by an intense laser beam. This causes interdiffusion of the well and barrier materials within the illuminated spot, which leads to modulation of the thickness of the quantum well and creation of dots [25]. A completely different method - selective epitaxy - involves growing a bulk substrate of the barrier material with a mask on its surface. Then, using lithographical methods, one creates small openings in the mask, and then one deposits the material of the quantum well. The well material will adsorb on the substrate only in the openings, so, as a result, we obtain an array of small islands [45, 73].

Although using all these methods it is possible to obtain QDs in a variety of shapes and sizes, recent years have brought new techniques, allowing for far more advanced QD engineering. I will cover in detail three such techniques: gated QD devices, growth of QDs by self-assembly, and fabrication of quantum rings by lithography and etching.

1.3.1 Gated quantum-dot devices

This type of QD design is particularly important in the context of my research into electronic correlations. In this design the potential of the nanostructure confines only one type of carriers, i.e., electrons, and the number of confined carriers is controlled electrostatically by applying voltage to metallic gates. The experimental technique most frequently used to probe these dots is transport spectroscopy, in which information about the system is derived from the properties of tunnelling current induced to flow through the device. I shall discuss the principles of tunnelling spectroscopy in the next Section; now let us only describe how these devices are built and operated.

There are two variants of the design. In the first one the lateral confinement for electrons is created by means of material engineering (by lithography and etching techniques) and using a metallic gate to control electronic population of the system. The first such device was fabricated by Ashoori *et al.* in 1992 [9], and the properties of the system of electrons localised on it were analysed theoretically by Hawrylak in 1993 [51]. Another device was created by D.G. Austing in the group of Seigo Tarucha at NTT Japan [4, 11, 92, 121, 122].

Here the gates are used not only to induce the tunnelling current, but also to change the lateral confinement of electrons by squeezing them electrostatically to a smaller area. The common feature of both designs is the fact that the tunnelling current flows vertically, i.e., along the axis of rotational symmetry of a disk-like quantum dot. This is why these structures are called **vertical quantum dots**. Let us briefly describe the second of the two devices.

A SEM micrograph and a schematic diagram of the sample is shown in Fig. 1.3. Its most important part, providing the vertical confinement for electrons, is the double-barrier heterostructure (DBH) seen in the centre of the diagram; the lateral confinement is produced by the lateral surface of the pillar and controlled by the gate. The sample is composed of the following elements. The substrate material is the n-doped GaAs, seen at the bottom of the diagram. Doping introduces electrons into the conduction band of this layer, so that we have mobile carriers that can be injected into the quantum dot. On top of this substrate the DBH is created using epitaxy. Each of the two barriers (denoted by darker regions in Fig. 1.3) is made of $Al_{0.22}Ga_{0.78}As$; the thickness of bottom barrier is 7.5 nm, and that of the top barrier is 9.0 nm. The material of the 12.0-nm-thick well between the barriers is $In_{0.05}Ga_{0.95}As$; the small amount of indium present in this layer causes the edge of its conduction band to be below that in the GaAs substrate. The DBH is then covered by a thick layer of n-doped GaAs, on top of which a metallic gate is deposited. A pillar, with the radius of about 0.5 μm, is formed using lithography and etching, and

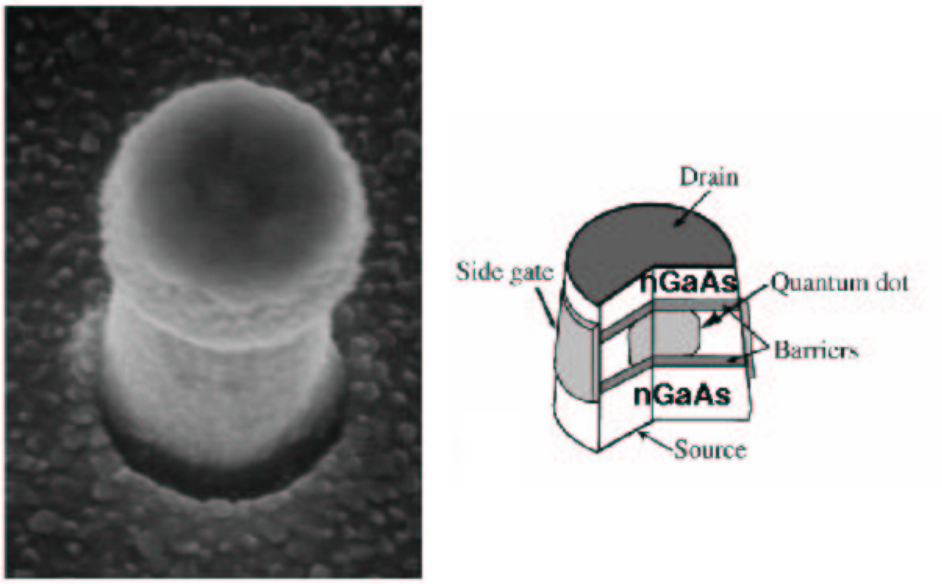

Figure 1.3: SEM micrograph of the vertical quantum dot device and a schematic diagram of the structure of the sample (Adapted from Ref. [123])

a metallic gate is also deposited on the lateral surface of the pillar, close to the DBH. In the tunnelling experiment a small voltage is applied to the top gate, which causes the electrons from the bottom nGaAs layer (the *source*) to tunnel into the dot and out to the top nGaAs layer (the *drain*). The tunnelling current is measured as a function of the voltage on the side gate and typically as a function of an external magnetic field applied along the rotational symmetry axis of the system.

Let us now move on to the second design of gated QDs: the **lateral gated quantum-dot device**. I am aware of several experimental groups working with the lateral dots, for instance the groups of Charles Marcus [81] and Robert Westervelt [129] at Harvard University, Marc Kastner at MIT [63], Klaus von Klitzing at MPI Stuttgart [66], and Leo Kouwenhoven at Delft in the Netherlands [68]. Here, however, I shall present a device built by A.S. Sachrajda and co-workers in the Quantum Physics Group at IMS NRC [31, 32, 33], because it was used to obtain experimental verification of my theoretical

results. To the best of my knowledge, this was the first device in which the number of confined electrons was known and controlled (from zero to about fifty). This was also the first device whose design allowed for the spin blockade spectroscopy (I shall describe this spectroscopic technique in detail in the next Section).

Fabrication of the lateral QD device consists of two stages. The first stage involves epitaxial growth of a GaAs/AlGaAs heterojunction. A schematic diagram of the sample composition is presented in Fig. 1.4(a). First, a thick (1-3 μm) layer of GaAs is deposited epitaxially on a substrate. Then, a heterointerface is formed by depositing undoped AlGaAs on top of the structure. The growth of AlGaAs is terminated after reaching the optimal spacer thickness, marked in Fig. 1.4(b) by the vertical line. Thicker n-doped AlGaAs and GaAs layers are subsequently deposited on top. This growth sequence results in the alignment of the conduction band edge shown in Fig. 1.4(b). As we move within GaAs along the z axis, closer and closer to the AlGaAs material, we see conduction band bending and formation of a triangular quantum well at the interface. This well is filled with electrons coming from ionised donor atoms (white circles). The well is narrow enough so that the electrons populate only its lowest subband. The spacer, made of undoped AlGaAs separates the doped AlGaAs region from the interface to insure high quality of the 2DEG in the well (and, in particular, high mobility of electrons).

The triangular quantum well at the interface confines the electrons only in vertical direction (along the z axis). The lateral confinement, i.e., the confinement in the plane of the 2DEG, is created by means of metallic gates, deposited lithographically on the surface of the sample. A scanning electron micrograph of the gates is shown in Fig. 1.4 (c). In this design there are typically four gates. The two large side gates and the small top gate provide the electrostatic lateral confinement, while the small bottom gate (the "plunger" gate) serves to tune the QD energy spectrum in the tunnelling experiment. Under negative voltage, all of these gates create an electrostatic potential, which propagates down to the 2DEG layer and depletes it locally of electrons, forming a soft lateral confinement, whose

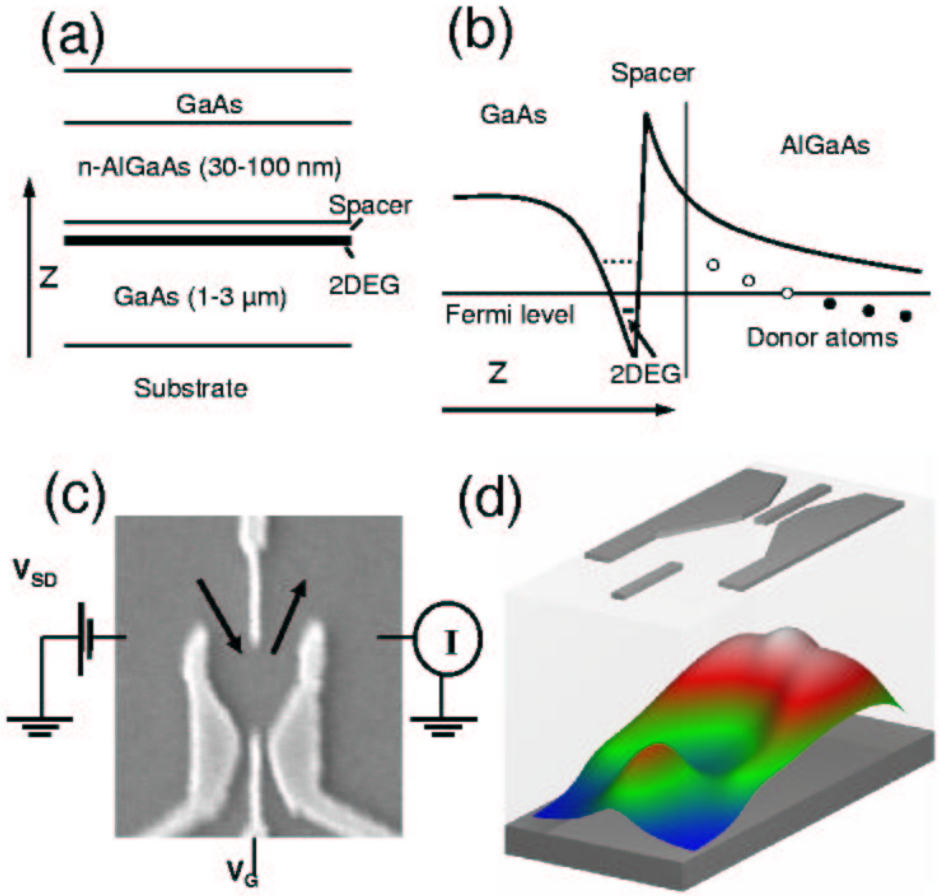

Figure 1.4: (a) Composition of the GaAs/AlGaAs heterojunction with the 2DEG. (b) Profile of the edge of the conduction band along the growth axis of the heterojunction. (c) Scanning electron micrograph of the surface of the sample with metallic gates. (d) Calculated electrostatic potential created by gates as experienced by electrons in the 2DEG layer (Parts (a) and (b) adapted from Ref. [116]; part (c) courtesy of A.S. Sachrajda at IMS NRC)

size is of order of 0.5 μm. This electrostatic potential, calculated [70] for typical gate voltages, is shown in Fig. 1.4(d). By tuning the gate voltages one can empty the dot of electrons, and then add them, one by one, in a fully controllable manner [31].

In this design, the source and the drain are the 2DEG electronic reservoirs to the left and to the right of the QD, so that the external voltage is applied laterally across the device, as shown in Fig. 1.4(c). Electrons tunnel in and out of the QD across the quantum point contacts defined by the top gate and one of the side gates, respectively (along black arrows in Fig. 1.4(c)). The tunnelling current is measured as a function of the voltage on the plunger gate V_G and the magnetic field perpendicular to the device. The function of this gate is to change the QD size by pushing it towards the top gate (increasing the slope of the large potential maximum shown in Fig. 1.4(d)).

In the lateral design the current tunnelling through the QD can be made to be spin-polarised. This occurs when an external magnetic field is applied perpendicularly to the surface of the sample (i.e., perpendicularly to the 2DEG). Note that the left and right reservoirs of electrons (the source and the drain) are both 2DEGs, and the tunnelling of electrons into and out of the QD involves the 2DEG edge states. Upon application of the external magnetic field, the Zeeman energy distinguishing between the two spin species translates into spatial separation of these edge states, so that the states close to both point contacts carry predominantly electrons with the same spin [31]. It is possible for electrons with the opposite spin to tunnel into the QD, however the probability for this to occur is small due to the fact that these electrons have to tunnel through a wider barrier. The spin-polarised injection and detection of the tunnelling current will play a major role in one of the main chapters of this thesis.

Note that the vertical device maintains a good circular symmetry irrespective of the potential applied to the side gate. The lateral device, on the other hand, produces a non-circular confinement, and the degree of this noncircularity varies with gate voltages. For these reasons, the shell structure of the single-particle spectrum of the QD can manifest

itself more clearly in vertical devices [121], while in the analysis of the results obtained with the lateral device the more complicated nature of the potential (due to its lower symmetry) often has to be taken into account [70].

The gated quantum-dot devices are relatively large (their typical size is of order of hundreds of nanometres), and therefore the shells of the single-particle energy spectrum are relatively close in energy (typical gaps are of order of several meV). These characteristic energies are smaller than the energy equivalent of the room temperature, and, in fact, the experiments on gated dots are usually conducted in millikelvin temperatures in a dilution fridge. The separation of single-particle states can be tuned by appropriately changing the voltage on the gates. Thus, the coefficient λ, defined in the beginning of this Thesis as the ratio of the characteristic interaction and single-particle energies, can be tuned as well, and one can obtain system with large electron-electron interactions. Due to the small interlevel gaps, the single-particle energy scale of the gated QDs can also be significantly tuned by an external magnetic field of order of several Tesla, leading to a nontrivial evolution of the system with the increase of the field. These issues will be discussed at length in this Thesis.

Gated quantum dots are also interesting in the context of the single-electron transistor [64] and Kondo physics (see Refs. [47, 117] and references therein). Finally, gated QD devices are seen as extremely promising candidates for quantum bits and quantum logic gates in quantum computing proposals. The most important theoretical paper in this field was published by Loss and DiVincenzo in 1998 [79]. In it, the authors consider using coupled gated QD devices to create entangled states of electrons.

1.3.2 Self-assembled quantum dots

Let us now move on to describing a different type of QD design, leading to formation of a confinement trapping both electrons and holes, and based on the self-assembly process. Self-assembly of QDs can be achieved by exploiting the Stranski-Krastanow phase tran-

sition occurring in the growth of highly strained semiconductor heterostructures [118]. I shall describe some details of this procedure following Petroff and DenBaars [98].

Let us consider a situation when a crystal of one semiconductor material is grown epitaxially on the surface of another material, and these two materials differ in their lattice constants. If this difference is very large, the deposited material will form an epitaxial layer full of crystallographic defects. However, if this difference is of order of 1-10%, the deposited material will initially form a layer of good quality, but highly strained. The degree of strain will increase as the layer becomes thicker, and, upon reaching a critical thickness (usually of order of a few monolayers), the planar growth of the layer will stop, and small islands of deposited material will start forming on top of the residual "wetting layer". This is the Stranski-Krastanow phase transition. The growth that follows this transition is a kinetic process driven by the strain energy. To minimise this energy, the material from larger dots will tend to diffuse along the wetting layer towards the smaller dots, thus leading to a better uniformity of the island sizes. If we deposit more material, it will also diffuse and end up being incorporated by the islands, which will grow both in height and diameter. Having obtained islands (dots) with desired dimensions, one can interrupt the growth and cap the structure with a "cladding layer" of the substrate material.

The islands will function as QDs only if the substrate material has a higher bandgap than the island material. In this context, GaAs or $Al_xGa_{1-x}As$ is frequently used as the barrier, on top of which $In_xGa_{1-x}As$ or $In_yAl_{1-y}As$ is deposited to form dots. Depending on molar fractions, the lattice mismatch between the barrier and dot materials is of order of 1-8%, making it possible to grow high-quality self-assembled dots (SADs). For example, the change from the two-dimensional to the three-dimensional growth mode upon reaching the critical thickness is illustrated in Fig. 1.5. In this case InAs is being deposited on the GaAs substrate, and the critical thickness of the dot material is about 1.7 monolayers. Dots seen in Fig. 1.5 have diameters of order of 30 nm $\pm$5% and heights of order of 10 nm

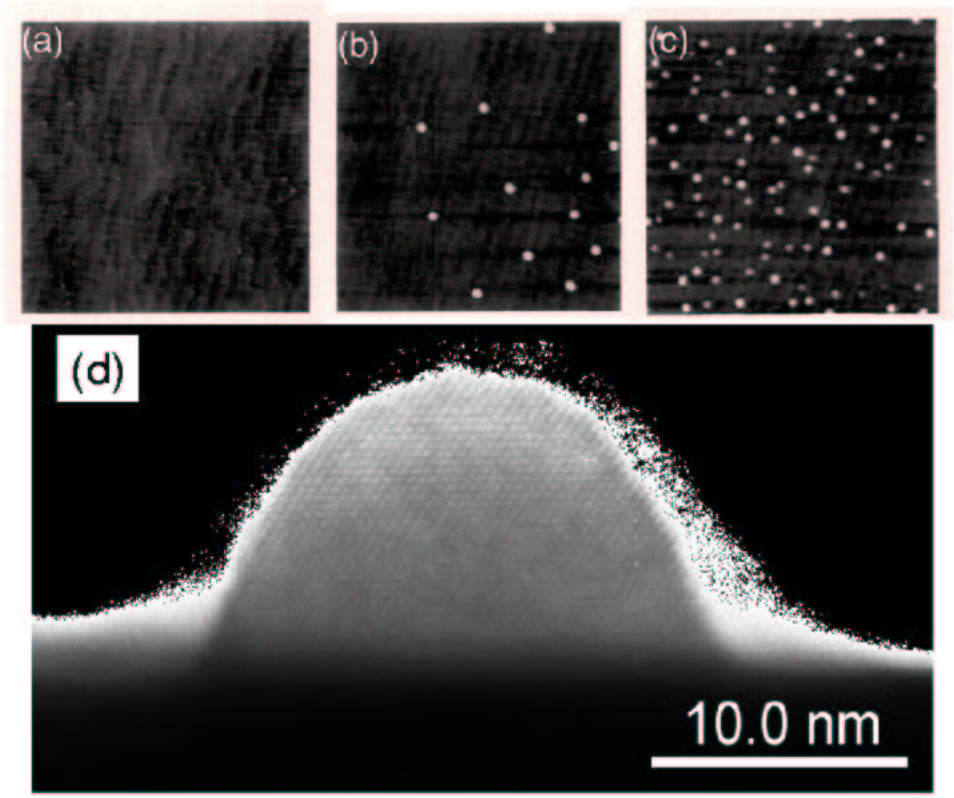

Figure 1.5: Atomic force micrographs of InAs self-assembled quantum dots for InAs coverage of 1.6 (a), 1.7 (b), and 1.8 monolayers (Adapted from Ref. [98]). Figure (d) shows a transmission electron micrograph of an InAs SAD (photo courtesy of J.P. McCaffrey at IMS NRC [85])

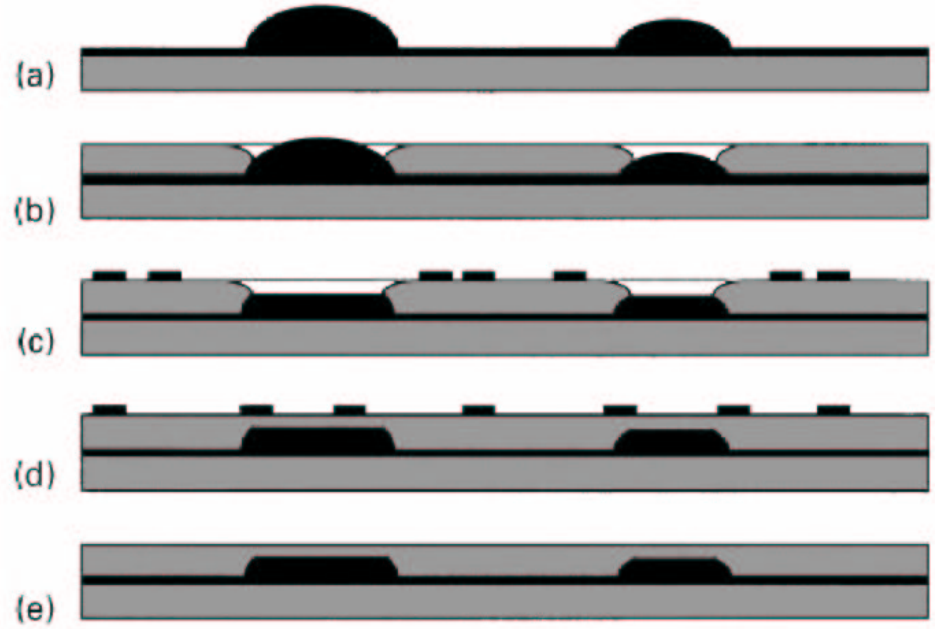

Figure 1.6: Growth of quantum disks using the indium flush technique (From Ref. [126])

±4%. Additionally, in Fig. 1.5 (d) I show a transmission electron micrograph of a SAD grown at the Institute for Microstructural Sciences, NRC Canada.

By choosing the misfit strain one can tune the sizes of SADs, since a smaller misfit leads to a smaller amount of strain, larger critical thickness and, ultimately, larger dots. Also, depending on the conditions of the growth itself, one can obtain SADs in a variety of shapes (e.g., pyramids with a square base [82], lenses [41, 101], hemispheres with hexagonal base [98]).

In recent years, Wasilewski *et al.* at IMS [126] developed a technique allowing for further control over the shape of SADs. The sequence of sample processing steps in this method is shown schematically in Fig. 1.6. First, SADs are grown in the Stranski-Krastanow mode along the lines laid out above, and in this example InAs is used as the dot material. As already mentioned, this growth leads to the formation of an array of dots with similar, but not identical diameters and heights, as shown in Fig. 1.6 (a). Then, the cladding layer is deposited on top of the sample, but this growth is interrupted, so that

dots are not completely covered with the barrier material (Fig. 1.6 (b)). This situation is energetically unfavourable from the point of view of total strain energy, since the indium atoms on the still exposed surface of dots experience a large stress from the surrounding GaAs barrier material. To lower this energy, indium atoms begin migrating from the dots onto the cladding layer, and gallium atoms from the cladding layer onto the dot, which results in a decrease of the dot height and capping of all dots (Fig. 1.6(c) and (d)). Note that this process of migration of atoms results in truncation of dots to uniform height. The next step, called the "indium flush", involves increasing the sample temperature, so that indium deposited on the surface of the cladding layer is desorbed (Fig. 1.6(e)). As a result, one obtains an array of randomly distributed dots, with variations in diameter, but with uniform heights. The growth can be further continued, i.e., upon deposition of the layer of barrier material of chosen thickness, evaporation of InAs can start again. The process of island growth will then start again, but now positions of QDs in the new layer will be aligned with positions of QDs already grown. This is due to the strain field, created by the QDs, and propagating upwards through the cladding layer of the barrier material. Thus one obtains stacks of coupled quantum disks, shown in Fig. 1.7.

Typically, the SADs can confine both electrons and holes, making it possible to examine the many-body systems composed of particles carrying both positive and negative charges. These systems can be probed by optical spectroscopic techniques, which I will briefly describe later on. However, the interaction effects are difficult to resolve in sufficient detail when working with arrays of QDs presented in the above discussion. This is due to the fact that the sizes of all dots are not exactly identical, but rather form a narrow distribution. As a result, different dots have slightly different single-particle energy spectra, and the corresponding spectroscopic features, obtained as a superposition of signals from the entire array, are broadened (this effect is called "inhomogeneous broadening"). To eliminate this broadening, a single QD must be isolated for a spectroscopic study. There are several techniques which can be used to this end. One of them involves cover-

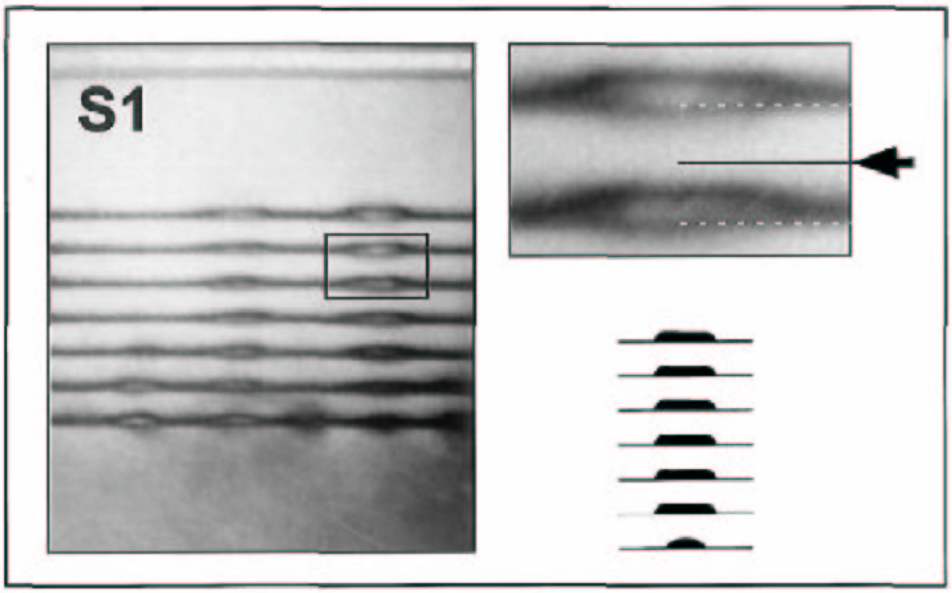

Figure 1.7: Cross-sectional TEM image of a stack of quantum disks grown using the indium flush technique. Image on the top right-hand side shows a magnification of the main micrograph (From Ref. [126])

ing the capped sample of the SAD array with a metallic thin film and creating openings in this film. If the opening is sufficiently small, it may be possible to address exactly one QD below. Another method involves covering a selected area of the QD array with a mask and etching away everything around it [14, 16]. This leads to a formation of a "mesa" structure, which, if it is small enough, may contain exactly one QD (or exactly one stack of QDs created using the indium flush method) in its interior.

Control over the position of a QD can also be achieved by patterning the substrate, on which the dots are grown. Here I shall describe a technique developed recently by Williams and co-workers at IMS [130]. The general principle of this method is illustrated in Fig. 1.8(a). First, a planar substrate (in this case InP) is grown as described previously. Then, a mask is deposited on top of the surface, and rectangular or square openings (with dimensions W of several hundred nanometres) are defined in it by lithography and etching (Fig. 1.8(a)). Then, deposition of the substrate material is resumed, but the material

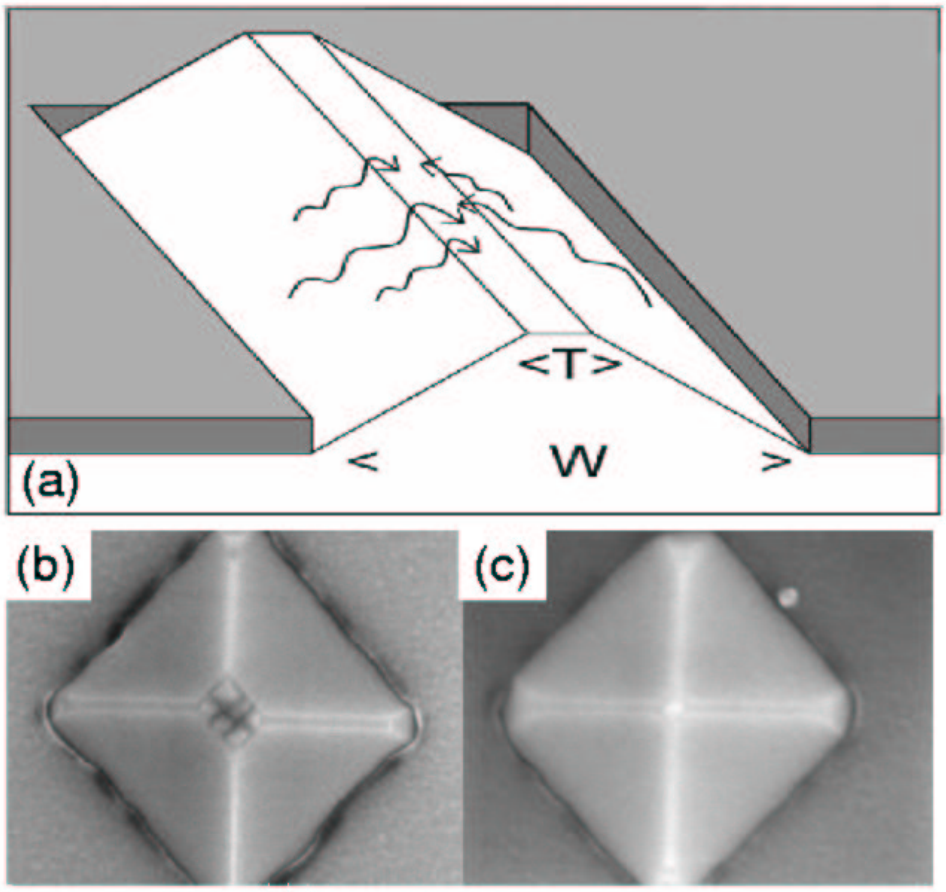

Figure 1.8: (a) Schematic illustration of the diffusion process in the growth on patterned substrates. This process leads to formation of templates, on top of which several (b) or only one quantum dot (c) can be grown. In these scanning electron microscopy images the base of the pyramid is 400 nm long (Adapted from Ref. [130])

adsorbs only in the openings. The substrate grows forming ridges or pyramids with walls corresponding to low-index crystallographic planes. This growth is continued until the width T of the area on top of the ridge is narrow enough to contain only one or two QDs. At this point the growth of the substrate is stopped, and deposition of the QD material begins. The QD material does not adsorb on top of the mask, and diffuses onto the sides of the ridge. However, the adsorption rate of the material to the substrate in this crystallographic orientation is very low. The deposited atoms continue diffusing across the structure, as shown in Fig. 1.8(a), until they reach the top of the pattern, where they finally adsorb.

Upon reaching the critical thickness the Stranski-Krastanow transition takes place, which leads to the growth of SADs on top of the pattern. As demonstrated in Fig. 1.8(b) and (c), the number of grown SADs depends on the size of the plateau. By careful engineering and growth control of the ridge it is possible to localise precisely one InAs SAD on top of the InP pyramid.

As mentioned before, QDs grown by self-assembly have diameters of order of a few tens of nanometres, and heights of a few nanometres. For typical materials used for barriers and dots, the depth of the confinement potential in the conduction band (or the height of the wall of the "quantum box") is of order of 600 - 800 meV. This means in practice that the lateral confinement of the QD is strong, and its single-particle energy spectrum consists of a small number of levels (typically fewer than 15), usually grouped into degenerate shells; the energy gaps between shells are of order of tens of meV. Introduction of charge carriers into such QDs can be achieved by optical excitation, but also by introducing doping in the barrier. The latter technique allows to fill QDs with electrons (or holes, depending on the kind of doping) without illumination. These systems are then ideal to study formation, dynamics and recombination of excitons and neutral or charged excitonic complexes (for reviews and references on that subject, see Refs. [62, 85]). Another important area of fundamental research involves enclosing such excitonic QDs in photonic cavities. In so

doing, both excitonic and photonic modes are confined and strongly coupled to each other (this is the Purcell effect [46]; for additional review and references see Ref. [55]).

The rapid progress in fabrication technologies of SADs is also driven by their possible applications, particularly in quantum optics. Single self-assembled QDs are used as detectors of infrared radiation (quantum dot infrared photodetectors, QDIPs) [10, 76], optical memories [97], single-photon sources [86, 88, 108] important for quantum cryptography [18, 24]. Arrays of SADs are also used as optically active regions in high-efficiency lasers. To date, successful prototypes of QD lasers have been demonstrated to work with low injection currents and high quantum efficiency even at room temperatures [42]. There are also proposals to use the intraband transitions in coupled QDs to generate terahertz radiation [5, 6, 131].

1.3.3 Quantum rings

I shall now describe another structure capable of confining electrons and holes, but with a topology different than that of the SADs - a quantum ring. The ring geometry is of interest, because it allows to access and manipulate the phase of a charge carrier confined in it by an external magnetic field, applied in parallel to the rotational axis of the system. As I will show later in this Thesis, this leads to the appearance of persistent currents and Aharonov-Bohm oscillations of the system's energy as a function of the number of flux quanta threading the ring.

Quantum ring nanostructures can be fabricated using self-assembly techniques [78], but here I will describe another method, involving lithography and etching. This is because I shall compare the results of my theoretical treatment of the many-body systems in the ring geometry to measurements performed on nanostructures obtained using this technique. My description follows that presented by Bayer *et al.* in Ref. [15]. A scanning electron micrograph of the sample is shown in Fig. 1.9(a). The inner radius of the sample is about 15 nm, while the outer radius is 45 nm. Composition of this sample is shown

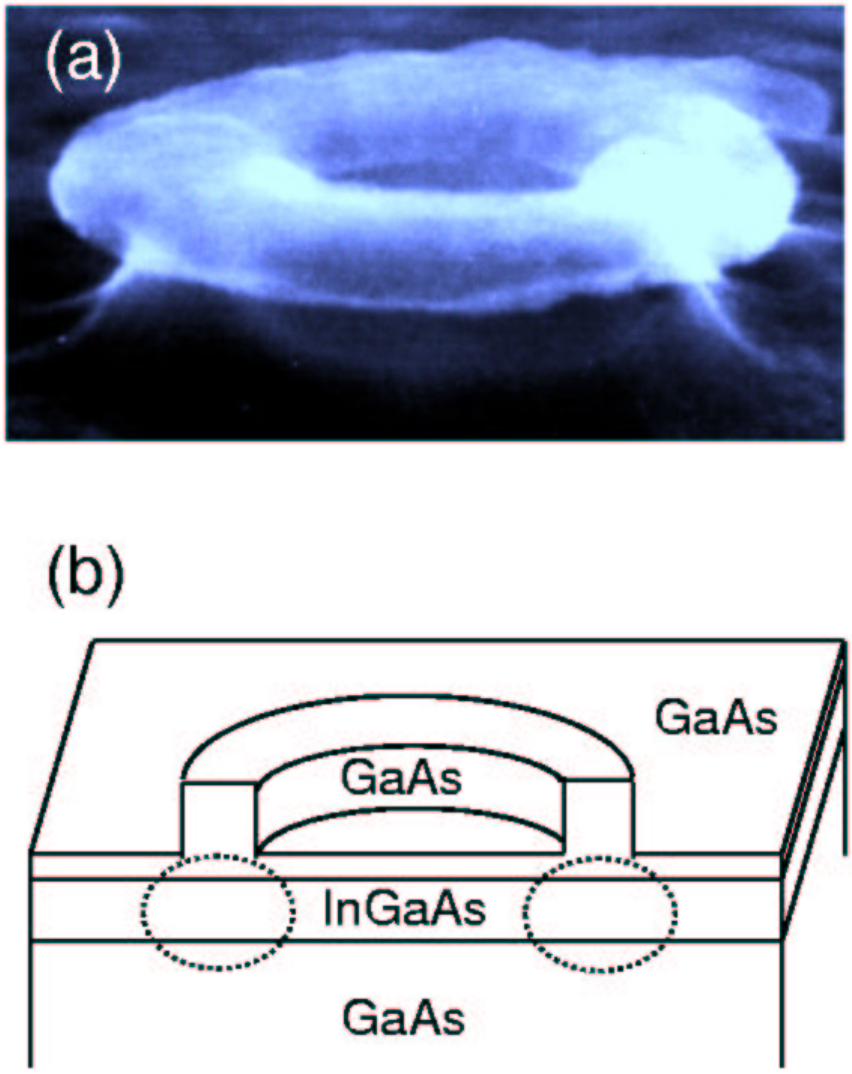

Figure 1.9: (a) Scanning electron micrograph of the quantum ring structure. The circular shape seen on top is the metallic mask produced by lithography before etching. (b) Schematic diagram of the structure; the carriers are confined in the areas marked by circles (Adapted from Ref. [15])

schematically in Fig. 1.9 (b).

To create the disk confinement, a 7-nm-thick layer of the $In_{0.1}Ga_{0.9}As$ quantum well material is lithographically deposited on top of the GaAs barrier material, and then capped by a 20-nm-thick layer of GaAs. Then, a ring-shaped metallic mask is deposited lithographically on top, and the structure is processed with etching. The etching removes only the GaAs material not covered by the mask and is stopped before reaching the InGaAs layer, so that the quantum well material is covered by a thin capping layer of GaAs everywhere except under the mask, where the GaAs layer is thick.

Let us now describe how the lateral confinement is formed. In regions where the GaAs layer was etched, the band profile along the vertical direction corresponds to an InGaAs quantum well with asymmetric barriers: on the bottom side of the well we have the GaAs material, but on the top side we have a very thin layer of the barrier material followed by vacuum. On the other hand, in the region underneath the GaAs ring the InGaAs well has a symmetric profile, being surrounded by a thick layer of GaAs material on both sides. The difference in height of the top barrier (very high in the etched area, lower under the GaAs cap) and the additional strain field produced by the GaAs ring creates a shallow lateral confinement, with a height of a few tens of meV, inside the InGaAs well. Note that the carriers are confined *not* in the ring structure seen in Fig. 1.9 (a), but rather underneath it (in the regions marked with circles in Fig. 1.9 (b)).

The control over ring radius R in the experiments with magnetic field is of particular importance. I will show in Section 2.3 that the magnetic field enters the single-particle energies in the system through the number of flux quanta $N_\phi \sim \pi R^2/\pi\ell^2$, where $\ell \sim 1/\sqrt{B}$ is the magnetic length. Thus N_ϕ depends linearly on the magnetic field, but the proportionality coefficient scales as R^2. For rings with large radii it is thus sufficient to use small magnetic fields to obtain large values of N_ϕ. On the other hand, the radii should be sufficiently small to produce distinct quantisation of single-particle energy levels. The rings fabricated by lithography and etching can be easily engineered to satisfy all these

conditions, since their radii can be naturally varied over a wide range by depositing a smaller or larger metallic mask. However, the existence of open surfaces appears to worsen the optical quality of the structures. This problem does not appear in self-assembled rings [78], but here the control of their shapes and sizes is much more difficult.

1.4 Spectroscopy

In the previous Sections I have described how the semiconductor quantum dots are created and how they can be populated with carriers. I will now move on to describing how these systems can be probed experimentally and how to interpret the results of these measurements. Understanding of these issues is important, since I seek experimental verification of my theories.

In this Section I shall describe two spectroscopic techniques. The first one - the photoluminescence spectroscopy - is used to study the electron-hole systems confined in quantum dots and rings. The second technique - the tunnelling current spectroscopy - is used to probe the many-electron systems confined in gated quantum dots, and I will discuss it in the particular case of the lateral QD design.

1.4.1 Photoluminescence experiment

As already mentioned, the self-assembled QDs and quantum rings are typically capable of confining both electrons and holes. That is why the experimental tool most commonly used in their study is photoluminescence (PL) spectroscopy. Here I shall describe only its fundamental principles; the interested reader will find reviews and references in Ref. [62, 85].

In order to obtain the PL signal, the QD must be first populated with electron-hole pairs (excitons). This is achieved by illuminating the sample with photons, whose energy is sufficient to promote electrons from the valence band to the conduction band in the barrier

material. Electrons and holes thus created diffuse across the sample and become confined in QDs, creating a system of many, strongly interacting charge carriers of both signs. The number of carriers trapped inside the QD depends on the power of the exciting laser. These complexes have a finite lifetime, since electrons will recombine with holes to lower the total energy of the system. In the absence of non-radiative recombination centres, such as impurities, the electron-hole pairs recombine radiatively, emitting photons, which are detected.

Information about the properties of the many-exciton system is obtained from the analysis of energies of the emitted photons. The emission spectrum of a dot with N excitons is given in by the Fermi's golden rule, which, in the dipole approximation, can be written as

$$A(\omega, N, i) = \frac{2\pi}{\hbar} \sum_f |\langle f, (N-1)|e\hat{\mathbf{e}} \cdot \mathbf{r}|i, N\rangle|^2 \delta(E_i - E_f - \hbar\omega), \tag{1.10}$$

where $\hat{\mathbf{e}}$ is the polarisation of the photon. Here, $|i, N\rangle$ denotes the initial state of the N-exciton system. On the other hand, $|f, (N-1)\rangle$ denotes the final state of the $N-1$-exciton system, which remains after the recombination of a single exciton. Note that the state $|f, (N-1)\rangle$ can be the ground state or one of the excited states of $N-1$ excitons. Due to the delta function in the above formula, the energy $\hbar\omega$ of detected photons, or the position of the PL peak on the energy axis, is equal to the energy difference between the initial state $|i, N\rangle$ and one of the final states $|f, (N-1)\rangle$.

The dipole matrix element present in the above formula gives the intensity of each emission line. The magnitude of this element depends on the initial and final wave functions of the system. Thus, the height of PL peaks provides information about the symmetries of many-particle wave functions, complementing the information about their energy, derived from peak positions.

The PL spectroscopy of single QDs is described in great detail in articles by Bayer *et al.* [16] and Hawrylak [50]. In these papers the authors model the systems of interacting electrons and holes in the absence of the magnetic field, and identify how these interac-

tion manifest themselves in PL spectra. A detailed analysis of interactions in excitonic artificial atoms in a magnetic field is given in Ref. [34], where the magnetic-field-induced degeneracies in the single-particle energy spectrum allow the study of interactions in the context of the so-called "hidden symmetries".

1.4.2 Tunnelling experiment

Let us now move on to describing the tunnelling current spectroscopy. This technique is used to examine the properties of many-electron gated quantum dots, and I shall describe how it is applied to lateral devices.

In Section 1.3.1 I have described that the lateral QD is created electrostatically by locally depleting the 2DEG of electrons. The 2DEGs on either side of such local lateral confinement are reservoirs of electrons. Upon application of a small voltage across the device, the electrons from, say, the left lead - the source - can tunnel into the dot, then tunnel out on the other side of the device and be collected by the other 2DEG - the drain. Since the tunnelling electron experiences the repulsion of all electrons already confined in the dot, this type of spectroscopy is called the Coulomb blockade (CB) spectroscopy. A detailed review of this experimental technique can be found in Ref. [69], here I shall only summarise its most important properties. My description follows that of Sachrajda *et al.* in Ref. [107].

In Fig. 1.10 I present a schematic diagram of the lateral quantum dot device. The two tall tunnelling barriers are created by the side gates of the lateral device. The plunger gate, represented by the voltage symbol V_P, is used to adjust the confinement of the dot, thereby shifting the QD states with respect to the Fermi energy μ_L of the source S and drain D.

Inside the dot there are several states lying below the Fermi level of the leads and occupied by electrons (full circles), and several states lying above μ_L and unoccupied (empty circles). In the simple charging model, the gap between the last occupied and the

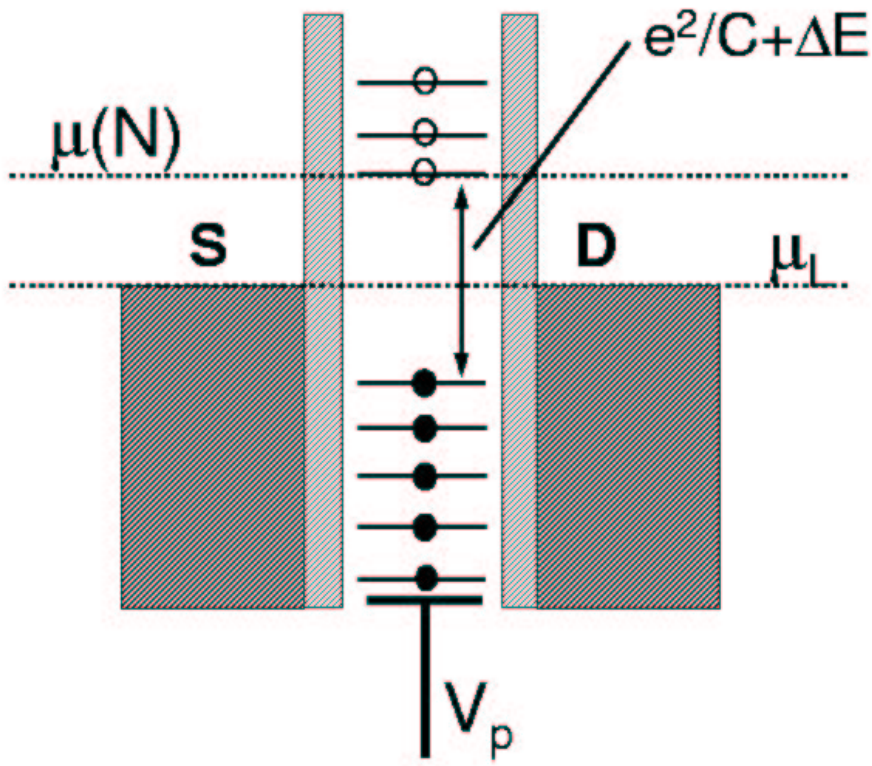

Figure 1.10: Schematic representation of energy levels in the lateral quantum dot (see text for details) (Adapted from Ref. [107])

first unoccupied QD level is equal to $e^2/C + \Delta E$, where C is the total capacitance of the QD. The capacitance C describes the effects of interactions of electrons inside the dot with each other and with the environment. Thus, if one wants to add another electron into the dot, one has to overcome the charging energy e^2/C. In lateral devices considered here this energy dominates the energy landscape of the system. The energy ΔE reflects the characteristic properties of the QD spectrum, and contains terms due to the discrete nature of QD single-particle states, effects of exchange and correlations. The goal of this technique is to examine the dependence of this term on the parameters of the system: confinement, external magnetic field, number of electrons.

Let us now formulate the conditions that have to be fulfilled for the current to flow. Let us denote the total energy of the system of n electrons in the left lead (the source) by $E_L(n)$, and the total energy of the system of N electrons in the quantum dot by $E_{QD}(N)$. The tunnelling of a single electron will be observed only if in this process the total energy of the leads plus total energy of the QD is conserved, i.e., when

$$E_L(n) + E_{QD}(N) = E_L(n-1) + E_{QD}(N+1). \tag{1.11}$$

Upon rearranging the terms in the above equation one gets

$$E_L(n) - E_L(n-1) = E_{QD}(N+1) - E_{QD}(N). \tag{1.12}$$

The left-hand side of this equation is the electrochemical potential of the lead: $\mu_L(n) = E_L(n) - E_L(n-1)$. Since the lead contains a very large number of electrons (of order of 10^{11}), this quantity does not depend on the number of electrons: $\mu_L(n) \equiv \mu_L$.

The right-hand side of the equation (1.12) is the electrochemical potential of the QD: $\mu_{QD}(N) = E_{QD}(N+1) - E_{QD}(N)$. It depends on the energy of the initial state of the system (with N electrons) and on the energy of its final state (with $N+1$ electrons), and thus carries information about the many-particle properties of the system of many interacting electrons confined in the device. The electrochemical potential $\mu_{QD}(N)$ is a discrete function of the number of electrons and a smooth function of the plunger gate

voltage V_P.

Let us now consider the alignment of energy levels presented in Fig. 1.10. In this case the electrochemical potential of the lead falls in the middle of the Coulomb gap between QD states. Thus the current cannot flow due to the Coulomb blockade. However, by tuning the plunger gate voltage V_P the electrochemical potential $\mu_{QD}(N)$ of the QD can be shifted down, and, for some gate voltage, aligned with the Fermi level μ_L of the leads. If this alignment is achieved, one electron from the source can tunnel back and forth through the left barrier. In the Fig. 1.10, to the right of the QD we also see the drain, whose Fermi energy is equal to that of the source. Therefore, upon alignment of all electrochemical potentials the electron will be able to tunnel from the source through the dot to the drain. If a small voltage is applied across the device (between the source and the drain), this tunnelling can be detected as a current flowing through the dot. Thus, if the current is measured as a function of the plunger gate voltage, one registers a series of peaks for voltages V_P, for which the electrochemical potentials are aligned. In such instances the number of electrons on the dot is undetermined. For the intermediate voltages, for which the condition (1.12) is not satisfied, the current is blocked, and the QD contains a well-defined number of electrons.

A typical addition spectrum, i.e., the current measured as a function of the gate voltage, and additionally as a function of the magnetic field, is presented in Fig. 1.11. The gate voltage is shown on the vertical axis, and the magnetic field - on the horizontal axis. One sees a collection of lines, denoting peaks of the tunnelling current. Each consecutive line marks the fulfilment of the tunnelling condition for the QD electrochemical potential $\mu_{QD}(N)$ with one more electron confined in the dot. The lines exhibit a series of features (kinks), which are signatures of changes of the ground state of the N-electron dot or of the $N+1$-electron dot. My goal is to reproduce this structure of kinks theoretically.

Before I conclude this description, I shall mention two possible modifications of this experimental technique. I have described the principles of the CB spectroscopy in the

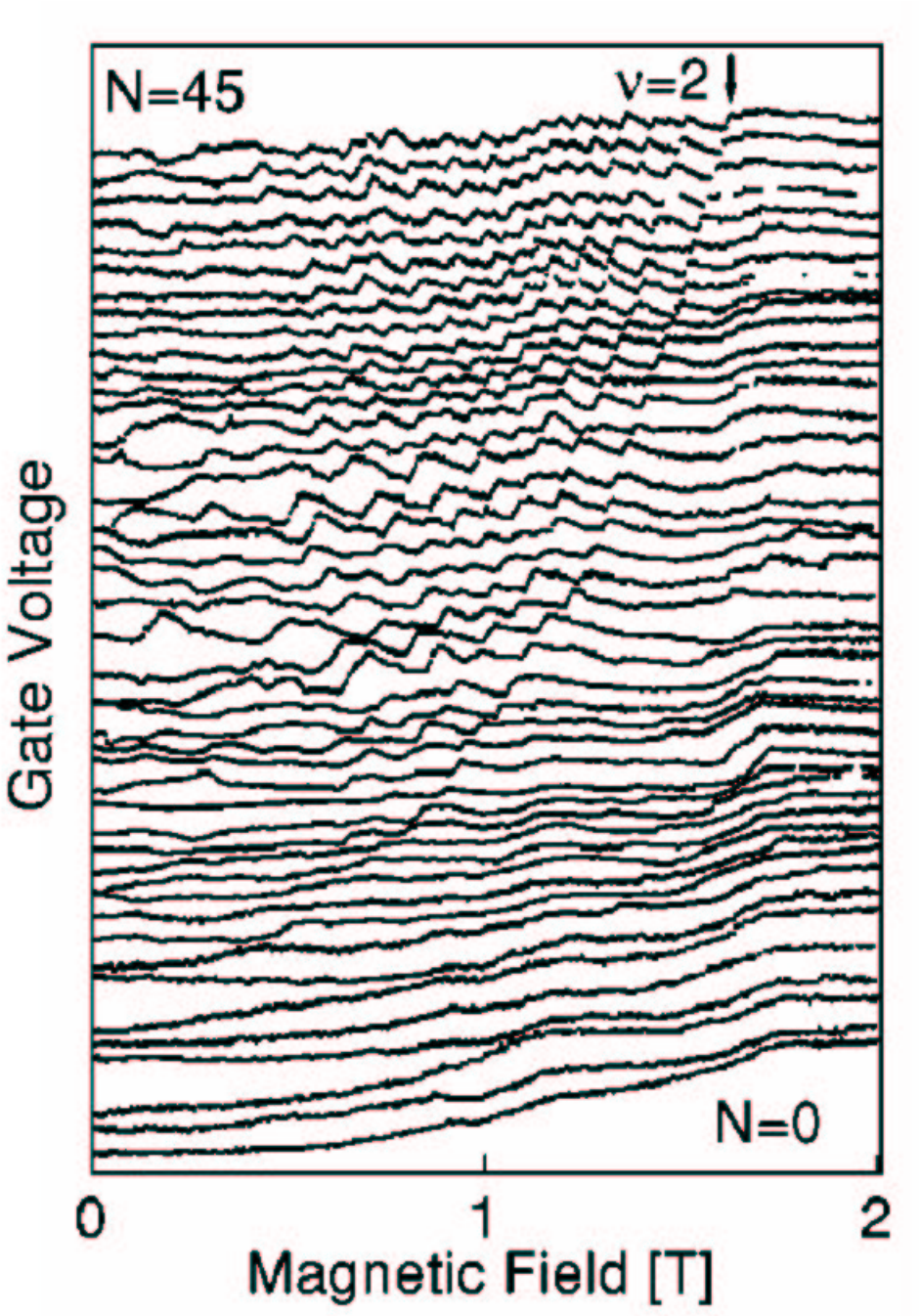

Figure 1.11: A typical addition spectrum of a gated quantum dot shown as a function of the magnetic field. Forty-five Coulomb blockade peaks are shown, with the charging energy manually removed (From Ref. [32])

low source-drain voltage regime, since I have assumed that the Fermi level of the source was aligned with the Fermi level of the drain. In this mode the tunnelling electron probes only the ground state of the $N+1$-electron dot. The spectrum presented in Fig. 1.11 was measured exactly in this mode, with the source-drain voltage of order of several μeV. However, a larger voltage (but smaller than the charging energy e^2/C) can also be applied across the QD. In this case the electron tunnelling from the source will probe not only the ground state, but also the excited states of the system. Also, on tunnelling from the QD to the drain, the electron may leave the N-electron dot in its ground or excited state. I shall compare my results to an experiment performed in this mode in one of the main chapters of this Thesis.

Up to now I have considered the electron tunnelling through the dot as a charged particle, experiencing the Coulomb repulsion from all the electrons confined in the dot. But this particle also has spin, and, as I have described in Section 1.3.1, in the case of lateral devices in an external magnetic field the tunnelling current consists predominantly of electrons with the same spin (say, spin down). In this case the fulfilment of the condition (1.12) is necessary, but not sufficient for the current to flow. The electrons will be able to tunnel onto the QD only if the final state of the $N+1$-electron dot can be created from the initial state of the N-electron dot by adding one electron spin down. If it is not possible, the current will not flow, and this phenomenon is called spin blockade. In practice the tunnelling current is not completely spin-polarised, and instead of the full spin blockade one only sees a modulation of the amplitude of the current. But this is sufficient to derive information about the spin of the system, which is complementary to that obtained from the positions of the CB peaks. Results of the spin-blockade experiments will also be discussed in this Thesis.

1.5 Electronic correlations in QDs: overview of the field and scientific contributions of this thesis

In the previous Sections I have defined the main subject of this Thesis: systems of many strongly interacting particles confined by semiconductor nanostructures. In particular, I am interested in identifying the manifestations of correlations, which requires a nonperturbative treatment, and comparing them to those of the direct and exchange Coulomb interactions, which can be captured by simpler mean-field approaches. I choose to treat interacting systems confined in nanostructures, because these systems can be probed experimentally both in the regime of strong and weak interactions, which allows to obtain experimental verification of my theories. This is possible because the properties of the atomic-like QD spectrum (in the language of quantum chemistry) or, equivalently, the QD DOS (in the solid-state terminology) can be *engineered*. There are several degrees of freedom: one can, within certain limits, change QD dimensions and symmetry, thereby influencing the energy separation and degeneracy of the single-particle states (separation and height of the DOS peaks) [11, 70, 105]. By building higher dots one can also bring the states belonging to the second vertical subband down in energy, thereby introducing new symmetry elements into the spectrum [58]. By choosing appropriate materials for the barrier and the well, one can tune the band offsets, thereby influencing the depth of the confinement, which gives control over the QD wave function penetration inside the barrier. Positioning two or more QDs close to each other allows for their quantum-mechanical coupling and leads to formation of an artificial molecule [2, 14, 96, 106, 114]. Finally one can also fill some types of QDs with a precisely known number of electrons. I will proceed by analysing the properties of the system of confined interacting particles as a function of these parameters, calculating characteristic quantities that can be measured, and comparing my results to the available experimental data, if such data exist. But, before I move on to discussing my results, I shall present a brief overview of the state of

scientific knowledge on the subject.

Collective behaviour of particles in strongly interacting systems leads to a number of nontrivial phenomena, from magnetism to superconductivity. Because of that it is not surprising that significant theoretical and experimental attention has been devoted to them for many years. Interest in collective phenomena in structures with lowered dimensionality has been particularly strong since 1982, when Tsui, Störmer, and Gossard [124] observed the appearance of unusual features in transport spectra of the two-dimensional electron gas under a magnetic field, interpreted as a new state of matter, whose appearance is due to electronic correlations. This effect, named fractional quantum Hall effect (FQHE), was intensively studied, both theoretically and experimentally (for reviews and references see a recent paper by Murthy *et al.* [89]). Here I shall mention two papers, written by Robert Laughlin [72], which opened the way towards theoretical understanding of the system and won their author the Nobel prize in 1998. In these papers the three-electron problem in a strong magnetic field is solved exactly with the assumption of a truncated Hilbert space. This solution is further extrapolated in a variational manner to systems with more electrons. As a result of these calculations, Laughlin postulated the existence of so-called incompressible correlated electronic states. He discusses one case in detail - the filling factor $\nu = 1/3$ phase, or, in other words, the case in which there are three magnetic flux quanta per each electron. In the words of Laughlin, these incompressible ground states of the system are "new states of matter", and they are somewhat reminiscent of the superconducting state in that they enable a dissipationless electrical conductivity. Laughlin predicted a series of such states decreasing in density and terminated by the Wigner crystalline phase.

Research into correlations in zero-dimensional nanostructures - quantum dots and rings - proceeds in several directions.

One direction of research involves examining properties of an N-electron system confined in a QD at zero magnetic field. The control parameter in this research is the ratio λ

of characteristic single-particle energy gaps to characteristic interaction energies, already defined in the beginning of this Thesis. Calculations in this domain were carried out using exact diagonalisation for $N = 3$, 4 [36, 87], and quantum Monte Carlo [40], spin density functional [102], and unrestricted Hartree-Fock theories for larger systems [133]. Mikhailov [87], for instance, finds that tuning the interaction parameter λ results in changes in the ground state of the three-electron system in a parabolic dot. If λ is sufficiently small, i.e., if the single-particle energy quantisation dominates the energy spectrum of the system, the ground-state configuration can be constructed by distributing the quasiparticles dressed in interactions on single-particle QD orbitals, subject only to the Pauli exclusion principle. In this regime the ground state of the three-electron system has total spin $S = 1/2$, since two electrons are placed on the lowest single-particle state with opposite spin, and one unpaired electron is confined on the first excited single-particle state. However, there exists a critical value λ_c of the interaction parameter, for which Mikhailov finds a transition in the QD ground state. The new ground state has maximal total spin possible, $S = 3/2$, and has the nature of a rotating Wigner molecule. This is demonstrated by examining the electronic pair correlation function, which appears to suggest that the electrons assume positions in the corners of a rotating equilateral triangle. Similar results are also obtained for larger systems [40, 102, 133]. I shall analyse transitions similar to those mentioned above, i.e., transitions from weakly correlated to strongly correlated phases of an electronic droplet as a function of the system parameters and the size of the Hilbert space in Chapter 4.

Wigner crystallisation is also observed in the presence of the magnetic field [48, 90, 119, 134]. Of particular interest is the case of the so-called maximum-density droplet (MDD), i.e., the system, in which all electrons are spin-polarised and occupy the consecutive single-particle orbitals on the lowest Landau level (in the language of the integer QHE, this is the $\nu = 1$ state). It has been shown [80], that this state is the ground state of the system for a finite region of magnetic fields. If the magnetic field becomes too low, electrons start

populating the Landau level with spin up. However, if the magnetic field is increased beyond the stability of MDD, holes appear in the centre of the dot, and the charge density of the system assumes the shape of a ring (falls to zero in the QD centre). This phenomenon was considered from the point of view of the Wigner crystallisation [48, 119]. In a study of pair-distribution functions derived from the ground states of QDs in high magnetic field, it was found that the structure of electronic quantum Wigner molecules is similar to the lowest-energy configurations expected for classical charged particles.

The second broad direction of research involves studies of magnetic-field evolution of electronic quantum dots. In the literature there is a large number of publications on the subject, presenting results of calculations carried out both at zero and finite magnetic fields using various methods: mean-field Hartree-Fock [17, 134], density-functional theory [11, 59, 75, 111, 128], quantum Monte Carlo [22, 49], and exact diagonalisation [54, 83]. All these methods suggest that for QDs with an even number of electrons there exists a region of magnetic fields, in which the ground state of the system is the so-called $\nu = 2$ spin-singlet phase in the terminology of the integer quantum Hall effect. Now, as the magnetic field is increased, one observes transitions in the ground state of the QD: electrons flip their spin one by one and the radius of the droplet increases until the fully spin-polarised maximum-density droplet is formed. If the magnetic field is increased even further, one expects the formation of QD-equivalents of incompressible states, discussed earlier in the context of the fractional quantum Hall effect. The sequence of spin flips can be completely understood without correlations, using simple arguments based on the competition between the single-particle energy quantisation and the interaction energies (direct and exchange). However, if correlations are taken into account, this sequence of phases turns out to be richer: the total spin of the system does not increase in the steplike manner, but rather exhibits oscillatory behaviour: each spin-flip event is preceded by a complete spin depolarisation. Similar spin oscillations take place also in the regime of magnetic field beyond the stability of the MDD: transitions between incompressible states

(fully polarised) are preceded by spin depolarisations. I find two theoretical treatments of these effects. First, presented by Imamura *et al.* [61], treats the correlated electron states in QDs as "electron molecules", which leads to interpretation of electronic spin wave functions as spin configurations in molecules, including the so-called resonating valence-bond states. The second treatment, put forward by Oaknin *et al.,* [91], describes the spin-depolarised states as spin-texture excitations (skyrmions), carrying topological and real charge equal to one. Excitations of the electronic droplet are thus charged skyrmions, which the authors express as condensates of interacting spin excitons. I shall discuss these phenomena in detail using the language of exact diagonalisation. This description, initiated by Hawrylak *et al.* in Ref. [53], will also include a discussion of stability of the correlated, spin-depolarised phases as a function of the system parameters (number of electrons, strength of confining potential, etc.). At this point I shall mention that in the experiments reported in literature the effects of direct and exchange Coulomb interactions were clearly identified [31, 33, 92, 121, 122], but, to the best of my knowledge, the spin depolarisations due to electronic correlations have not been accounted for. It is only in recent research, carried out by the Quantum Physics Group and the Quantum Theory Group (with the author of this thesis as a member) at the IMS NRC that these spin oscillations were clearly identified and traced back to the correlated behaviour of electrons confined in the lateral gated QD device (see Chapter 5).

Finally, the third research direction involves a specific type of correlations, manifesting itself in entangled states of systems of particles. The issue of entanglement is of particular interest for the rapidly developing field of quantum computation (see e.g. [43]). In quantum computers information is stored and processed using quantum bits (qubits), the quantum counterparts of classical bits. The difference between these two is such that classical bits can only store two states: $|0\rangle$ or $|1\rangle$, while qubits can be in any linear superposition $\alpha|0\rangle + \beta|1\rangle$, subject only to normalisation constraints. But information stored in the form of such quantum state has to be processed using quantum principles as well.

This is accomplished with quantum logic gates, built out of two coupled qubits; ability to perform single- and two-qubit operations is sufficient to build a quantum computer. It is said that the state of the system is *entangled,* if the total state of the array of qubits cannot be written as a simple tensor product of states of each individual qubit. If one-electron gated quantum dots are taken as qubits, as suggested by Loss and DiVincenzo [39, 79], the state of an array of such coupled qubits is thus a highly correlated state of many electrons. In this work I shall explore a different qubit design: as two qubits I will take an electron and a hole, both confined in the same double-dot structure, consisting of two vertically coupled self-assembled dots. I will show that the entanglement is created in such systems by the Coulomb electron-hole interaction (Chapter 6).

I shall also analyse the electron-hole correlations outside the context of quantum computation. In Chapter 7 I shall consider the problem of a negatively charged exciton (X^-, composed of two electrons and one hole) confined in a quantum ring and subject to an external magnetic field directed along the rotational axis of the ring. It is well known that the ground state energy of a single electron in this geometry exhibits the Aharonov-Bohm oscillations (for reviews and references see Ref. [27]). The X^- complex is charged (carries the charge of an electron), so one would expect this complex to exhibit the Aharonov-Bohm oscillations as well. As I shall demonstrate, this is true in the regime of weak interactions, i.e., when the radius of the ring is sufficiently small. In the regime of strong interactions the electron-hole correlations lead to suppression of the Aharonov-Bohm oscillations of X^-. Of interest is thus a photoluminescence experiment, in which the X^- complex recombines, emitting one photon and leaving one electron still confined in the ring. When calculated as a function of the magnetic field, the energy of such photon exhibits clear Aharonov-Bohm oscillations due to the oscillatory character of the energy of the final-state electron. Thus one can observe *optically* the oscillations of the energy of the *single electron,* and this is possible only due to the correlated character of the X^- complex.

However, before I can move on to considering all these problems, I must carefully introduce the tools of my analysis. I start by calculating the single-particle states of nanostructures with various geometries: parabolic and disk-shaped QDs and the quantum ring. Then I shall move on to describing selected computational methods of many-body physics capable of capturing the correlation effects. My method of choice is the exact diagonalisation technique. This approach involves three steps: construction of a basis set of the Hilbert space, writing the Hamiltonian in this basis in a matrix form, and numerical diagonalisation of this matrix. I shall describe each of these steps in detail. I shall also compare the exact diagonalisation with other computational techniques, such as the spin density functional theory and the quantum Monte Carlo approach.